

Elements for Plasmonic Nanocircuits with Three-Dimensional Slot Waveguides

By Wenshan Cai, Wonseok Shin, Shanhui Fan, and Mark L. Brongersma*

Over the last decade, the field of plasmonics has received significant attention for its ability to utilize engineered metallic nanostructures to manipulate the flow of light down to the deep subwavelength scale (see, for example, recent reviews^[1–4]). Extended metal structures can serve as compact optical waveguides that can transport information in the form of surface plasmon-polaritons (SPPs). Among the wide variety of plasmonic waveguiding geometries being investigated, planar structures consisting of one or more flat metal-dielectric interfaces (supporting single-interface SPPs, metal-dielectric-metal gap plasmons, long-range surface plasmons, etc) have received the most intensive study;^[5–7] their popularity arises from their fundamental physical importance as well as the relative ease of analyzing and modeling such two-dimensional (2D) structures. We note, however, that chip-scale photonic nanocircuits require that flexible routing of light occurs within a 2D platform, which implies that waveguides used for such on-chip optical links need to be three-dimensional (3D).

Among an expanding family of 3D plasmonic waveguides including nanoparticle arrays,^[8] metallic nanowires^[9] and V-shaped grooves,^[10] metallic slot waveguides, which consist of subwavelength slots in thin metallic films, represent a promising candidate for chip-scale nanocircuitry because of their tight mode confinement, reasonable propagating length and intrinsic broadband nature. This waveguide geometry also naturally lends itself to a wide variety of applications which require combined electrical and optical functions. For example, an electro-optic modulator based on a slot or gap plasmon waveguide can conveniently use the same metals to define an optical guide and the electrical contacts that generate an electric field across a switching medium.^[11] Although the general properties of such plasmonic slot waveguides have been investigated to a certain extent,^[12–16] a systematic study is still lacking for the basic building blocks necessary for the routing and manipulation of SPPs in 3D slot waveguides. In this work, we aim to analyze and optimize several fundamental elements for 3D plasmonic interconnects, such as mirrors, bends, and splitters.

We start our investigation with the mode characteristics of straight slots, including the mode index, loss factor, energy confinement as well as the spatial distributions of all the field components. Without loss of generality, in all numerical studies we use a representative wavelength of $\lambda_0 = 850$ nm that falls between the visible spectrum and the telecommunication region. We also choose a reasonable geometrical aspect ratio of the height ($h = 100$ nm) and width ($w = 80$ nm) of the slot; these dimensions are currently achievable with standard nanofabrication techniques such as electron-beam lithography, focused ion milling, and various etching processes. Silver with a permittivity of $\epsilon = -35 + 0.5i$ ^[17] is used for the metallic structure and the dielectric surrounding the metal is assumed to possess a refractive index of $n_d = 1.5$. Such a symmetric geometry supports a deep-subwavelength mode that has no cut-off, and is a true guided mode in the sense that its modal index is higher than that of all the surrounding media.^[14] We will call a waveguide with these parameters our “standard” 3D slot waveguide. To facilitate the understanding of the nature of the slot mode, we demonstrate the asymptotic behavior of 3D silver-silica slot waveguides as their dimensions approach those of 2D metal-dielectric-metal (MDM) waveguides or 3D waveguides supporting edge modes. We will refer to a 2D MDM waveguide with the same constituent materials and channel width w as the “2D reference waveguide” and use its properties for comparison purposes.

We first study the effective mode index and loss factor of the fundamental mode supported by a 3D metallic slot waveguide. **Figure 1a** and **1b** show the real and imaginary parts of the mode index for waveguides with varying slot width w . In order to reveal the asymptotic behavior of 3D slot modes, we include in **Figure 1** the mode indices of the 2D MDM waveguides mentioned before and 3D edge modes supported by a truncated metallic film, which is equivalent to one half of the slot waveguide with an infinite gap width. For both the 3D slot waveguide and its 2D planar counterpart, the mode index increases as the dielectric gap size shrinks due to a larger overlap between the plasmon modal profile and the metal. For the same reason the plasmon modes become more lossy for smaller slot width, as indicated by the imaginary part of mode indices in **Figure 1b**. The 3D slot plasmon asymptotically approximates the 2D MDM mode and the 3D edge mode when the slot width approaches the two limits of $w \sim 0$ and $w \sim \lambda_0$, respectively. For the representative waveguide with a slot size of $w \times h = 80 \times 100$ nm², the mode index is $n_{mode} = 1.96 + 0.0056i$, which implies a propagation length $1/\alpha = \lambda_0/4\pi\text{Im}(n_{mode})$ of ~ 12 μm .

In **Figure 1c** we plot the magnitude distribution of all electromagnetic field components of the slot SPP mode. Similar to the 2D reference waveguide, the central part of the slot eigenmode is quasi-TEM with a dominant vertical magnetic field H_y and a horizontal electric field E_x , along with a much weaker

[*] Dr. W. Cai, Prof. M. L. Brongersma
Geballe Laboratory for Advanced Materials
Stanford University
Stanford, CA 94305 (USA)
E-mail: brongersma@stanford.edu
W. Shin, Prof. S. Fan
E. L. Ginzton Laboratory
Stanford University
Stanford, CA 94305 (USA)

DOI: 10.1002/adma.201001440

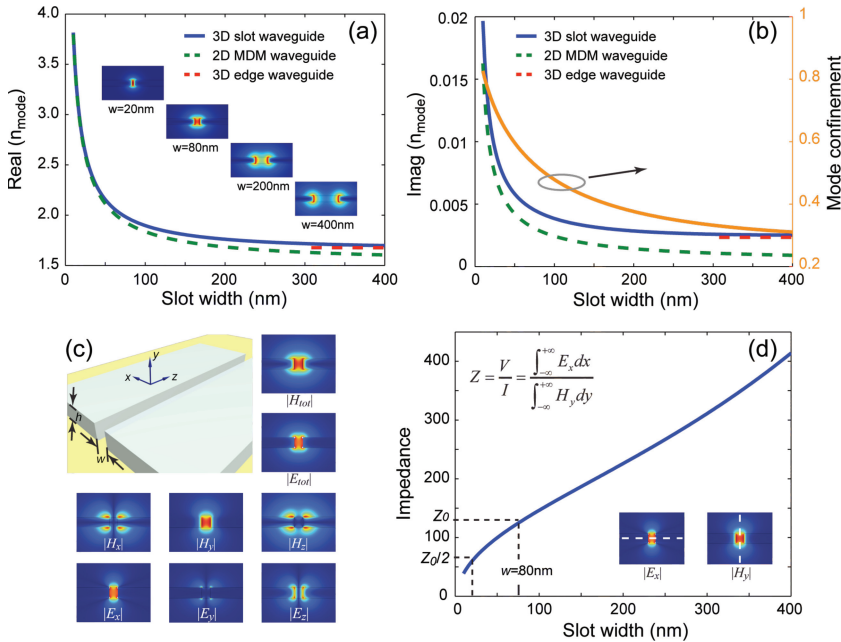


Figure 1. (a) Real part of the mode index of 3D slot waveguides and its asymptotic behavior. Inset: cross-sectional view of the magnetic field distribution for waveguides with a series of slot width. (b) Imaginary part of the mode index and mode confinement of a 3D slot waveguide. (c) Schematic of a representative slot waveguide and all field components of the eigenmode. (d) Characteristic impedance Z of a 3D slot waveguide obtained by direct field integrals. Inset: plots of the relevant fields and the integral paths used for estimating the slot waveguide impedance.

longitudinal field E_z bound to the metal-dielectric interfaces. The slot mode modestly extends around the edges and creates local hotspots around at the corners. These are typical features borrowed from the edge plasmon mode associated with a truncated metal slab. The size of the bound mode supported by the metallic nano-slot is deeply subwavelength, since a majority portion of the mode energy is localized inside the slot region. We define the mode confinement as the ratio between the electromagnetic energy within the $w \times h$ area and that of the entire slot eigenmode.^[14,15] The right axis of Figure 1b shows the energy confinement of the 3D waveguide as a function of slot width w for a fixed slab thickness of $h = 100$ nm. As expected, the SPP mode is better confined within the slot region for narrower channel width, as the structure asymptotically approaches its 2D counterpart with a mode confinement close to unity. The confinement factor is 0.52 for the 80×100 nm² standard slot waveguide.

Characteristic impedance models are commonly used in the microwave theory and provide a powerful tool for the analysis of waveguide branches. Strictly speaking, plasmonic waves in both 2D and 3D metallic waveguides are non-TEM modes, therefore voltage and current necessary for evaluating the impedance $Z = V/I$ cannot be unambiguously defined. Fortunately, the transverse electromagnetic fields (E_t and H_t) in 2D planar metallic waveguides are largely uniform and well confined in the dielectric region, which allows for the approximation of $V = wE_t$ and $I \propto H_t$.^[18] Consequently, an equivalent impedance proportional to both the mode index and the channel width can be defined, and has been successfully applied to the analysis

of 2D waveguide junctions and cascading problems.^[18,19] Such a treatment, however, is not applicable to 3D metallic slot waveguides due to their complicated mode profiles. In this work we evaluate the equivalent impedance by means of direct integrals of relevant field components, as the effective voltage and current are linked to the transverse fields E_x and H_y by $v = \int_{-\infty}^{+\infty} E_x dx$ and $I = \int_{-\infty}^{+\infty} H_y dy$.^[20] The integral paths are taken along the central cuts of the waveguide's cross section, as shown in the inset of Figure 1d. Based on this technique, we estimate the characteristic impedance of the standard 80×100 nm² slot waveguide to be $Z_0 = (129 + 0.3i) \Omega$. In Figure 1d we plot the real part of the equivalent impedance as a function of slot width w , which will later be used for the analysis of waveguide components such as an impedance-matched beamsplitter.

After the investigation of the general properties of straight metallic slot waveguides, we numerically study a number of passive building blocks employing such waveguides using a commercial finite element package Comsol Multiphysics. The devices are excited with the slot eigenmode obtained from boundary mode analysis, and all simulation domains are terminated with customized perfectly matched layers. In all numerical work,

SPPs are evaluated sufficiently away from waveguide junctions so that slot eigenmodes are fully formed, and the usual propagating loss between evaluation planes is compensated in order to reflect purely the characteristics of the passive components being studied. A general feature shared among all the building blocks defined using 3D slot waveguides is that their performance (in terms of pertinent efficiencies or coefficients) is always inferior to the planar 2D counterparts.^[18] The reason is rather straightforward. The 3D plasmonic waveguide is inherently an open system. Although the SPP eigenmode in a symmetric 3D slot waveguide is a bound mode that does not leak to metal slabs or ambient dielectric, any additional features in the slot waveguide can potentially incur energy leakage to multiple channels including 2D plasmon modes (the dominant factor), out-of-plane radiation, and local heating. For instance, a blocked channel in the 2D reference MDM waveguide represents a shorted load, which can be described by a zero impedance and therefore gives rise to a perfected reflection. In another word, an ideal mirror for the 2D MDM waveguide can be realized by simply blocking the dielectric gap with a metal. This seemingly trivial exercise, however, does not work for 3D slot waveguides. Full-wave electromagnetic simulations show that the power reflection from a blocked "dead end" in the 80×100 nm² slot waveguide is ~ 0.58 , far lower than the expected reflection level from a shorted load transmission line. It is worth noting that the obtained power reflection is reasonably close to the confinement factor that we discussed previously. This is a rule of thumb for estimating the reflection level from "dead end" mirrors in other similar slot waveguides as well.

Sharp bends in waveguides are basic components for high density integrated photonic circuits. One of the most intriguing aspects of 3D plasmonic waveguides is that they enable light to be routed around a 90° corner occurring at a subwavelength scale, a feature not available in either conventional dielectric waveguides or photonic crystal devices. In the 2D reference waveguide a right-angle bend gives rise to a reflection of ~0.14, which results from the deviation of the actual case from the quasistatic approximation ($w/\lambda_0 \sim 0$). Such an imperfection can be ameliorated by realizing a 90° waveguide bend with a constant channel width (and thus impedance) throughout the bend. Our full-wave simulation (not shown) confirms that the reflection can be suppressed to virtually zero along with a transmission of over 0.995 through the right-angle bend when a bending radius of 50 nm is used.

In marked contrast to the 2D structure, a sharp 90° bend in the standard slot waveguide exhibits a substantial loss of over 50% along with a pronounced reflection of about 16%. Consequently, a rather limited power fraction of ~28% is transmitted through this element. A full-wave simulation for the magnetic field distribution $|H_{tot}|$ for a sharp 90° bend in the standard waveguide ($w \times h = 80 \times 100 \text{ nm}^2$) is illustrated in Figure 2a, which shows a low power level in the output port and a clear standing wave pattern in the input branch due to the reflected SPPs from the junction. One way to improve the bending performance is to reduce the slot width w_{out} of the output waveguide. In Figure 2b we plot the reflection, transmission and loss from a waveguide bend for different output slot widths. When w_{out} is reduced to half of the input channel width, the reflection is suppressed to a minimum value of ~5% and a transmission of over 40% can be achieved. A more elegant method to eliminate the power reflection, similar to the situation with 2D MDM bends, is to introduce a bending

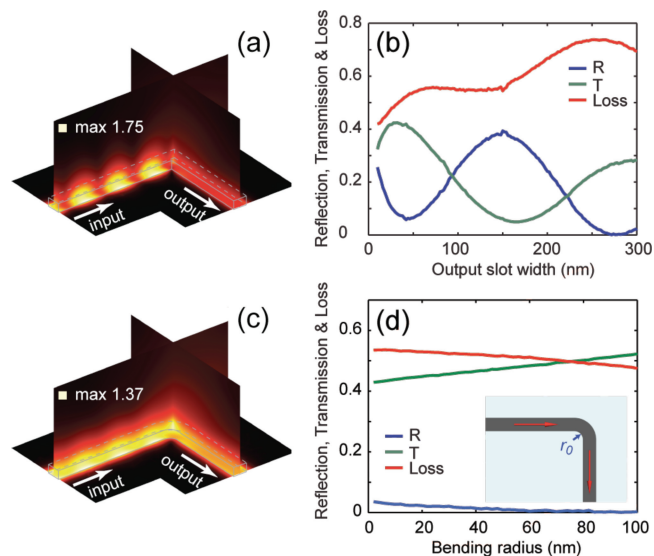


Figure 2. (a) Full-wave simulation for the normalized magnetic field distribution $|H_{tot}|$ of a sharp 90° bend in the standard slot waveguide ($w \times h = 80 \times 100 \text{ nm}^2$). Only the upper half of the structure is shown for symmetry reasons. (b) Transmission, reflection and loss of right-angle bends with varying output slot width. (c) Full-wave simulation of a smooth 90° bend with a bending radius of 50 nm. (d) Transmission, reflection and loss of 90° bends with varying bending radius.

curvature. The field mapping in Figure 3c shows that when a bending radius of 50 nm is used, the standing wave pattern in the input waveguide mostly disappears, and the power transmission through the bend reaches over 50%. We note that the introduction of bending curvature does not increase the footprint of the device, as the power reflection from the bend can always be efficiently suppressed regardless how small the bending curvature is. As long as the sharp outer corner of the bend is removed, the device performance is largely insensitive to the bending radius, as implied in Figure 2d.

T-shaped splitters are essential elements for power dividing and directional coupling in waveguides (Figure 3a). A T-splitter in the 2D reference waveguide directs ~42% of the input plasmon power into each output channel, and ~6% of the incident power bounces back from the junction. Unlike the right-angle bend in which the detrimental reflectance can be removed by using a bending curvature, a curved junction in a T-splitter does not eliminate backward power flow, as there exists a fundamental limit of $R_{min} = 1/9$ to the minimum power reflectance from a three-port junction of identical branches.^[21] When the slot width of output channels is allowed to vary, the reflectance from a T-splitter in a 2D MDM waveguide can be entirely eliminated by means of the impedance matching technique.^[18]

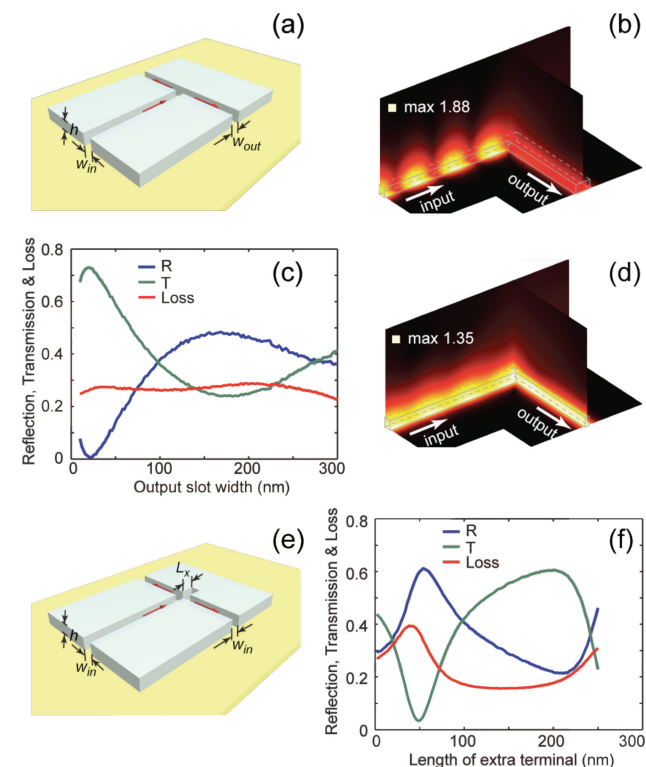


Figure 3. (a) Schematic of a T-splitter in a 3D metallic slot waveguide. (b) Full-wave simulation for the normalized magnetic field distribution $|H_{tot}|$ of a T-splitter for the standard waveguide ($w \times h = 80 \times 100 \text{ nm}^2$). Only a quarter of the structure is shown for symmetry reasons. (c) Transmission, reflection and loss of T-splitters with varying output slot width. (d) Full-wave simulation of a T-splitter with an optimized output slot width. (e) Schematic of a T-splitter in a 3D metallic slot waveguide using an extra terminal. (f) Transmission, reflection and loss of T-splitters with varying lengths of an extra terminal.

To test the feasibility of a reflection-free T-junction defined in 3D slot waveguides, we first simulated a 3D T-splitter in which all ports share the same cross-section of $w \times h = 80 \times 100 \text{ nm}^2$. A substantial reflection of $\sim 29\%$ occurs along with a mediocre transmission of $\sim 22\%$ into each output channel, as indicated by the magnetic field distribution $|H_{\text{tot}}|$ shown in Figure 3b. We can seek the optimal junction structure by scanning the slot width w_{out} of both output branches, as shown in Figure 3c. A minimum reflection of less than 1% occurs with an optimized slot width $w_{\text{out}} = 22 \text{ nm}$. This numerical optimization fits remarkably well with the impedance analysis that we discussed previously. Figure 1d shows that the characteristic impedance of the 3D slot waveguide drops monotonically when the slot width shrinks. In particular, compared to the input slot ($w_{\text{in}} = 80 \text{ nm}$) with an impedance of $Z_0 = 129 \Omega$, the characteristic impedance Z_{out} decreases by half when the slot width is reduced to $w_{\text{out}} = 22 \text{ nm}$. Since the two output branches of a T-junction can be visualized as a series combination, the equivalent load impedance $Z_L = 2Z_{\text{out}}$ matches perfectly the input impedance, which explains the near-zero reflection seen in Figure 3c. The drastic improvement can be clearly visualized in the field mapping shown in Figure 3d. When this optimized width of output slots is used, the standing-wave pattern in the input branch is substantially suppressed, and the combined power throughput through both channels reaches ~ 0.74 , a 70 percent improvement over the equal-width T-splitter.

If the waveguide geometry for a circuit is standardized at, say, $w \times h = 80 \times 100 \text{ nm}^2$ and does not allow for the change of output slots, a quasi-optimized T-splitter can be realized by gradually tapering the output channel width from the optimal value of $w_{\text{out}} = 22 \text{ nm}$ back up to the standard slot width of 80 nm . In this case the power reflection from the entire junction slightly exceeds the theoretical minimum of $R_{\text{min}} = 1/9$, and the transmittance through each output branch can still reach over 30%. There is yet another scheme to improve the performance of a T-splitter without the involvement of fabrication-challenging narrow slots. As shown in the schematic in Figure 3e, an extra terminal of length L_x can be introduced to control the interference behavior in the input branch. An improved performance of the T-splitter is expected when a destructive interference is obtained in the input channel. In Figure 3f we show the power transmission and reflection of the T-splitter as a function of the length of the extra terminal. An optimal length of $L_x = 200 \text{ nm}$ produces a combined output of $\sim 60\%$ along with a suppressed reflection of $\sim 20\%$. As a side note, we have also tested an X-junction where four identical 3D slot branches meet with 90° angle between adjacent channels. An equal power of $\sim 19\%$ is transmitted through each output channel, and the power reflectance back into the input port is about 34% (not shown). The total leakage loss of $\sim 10\%$ is a relatively small value compared to that of the bends and T-splitters that we discussed earlier, because in the 4-way junction we avoid the strong interaction between the plasmon wave and geometrical discontinuities such as a metallic edge or corner.

We note that the wavelength and geometrical parameters used in all the foregoing discussions correspond to a very representative case study, whereas various possibilities exist to improve the performance of these passive waveguide elements. For example, we expect better features at the important telecommunication

wavelength of $\sim 1.5 \mu\text{m}$ due to the combined effect of two reasons—the fraction of modal energy in metals reduces as the magnitude of negative permittivity increases, and the quasi-static approximation becomes more accurate when $\lambda_0 \gg w$. An improved performance can also be achieved if a slot of larger aspect ratio h/w is considered, which brings the situation closer to the 2D MDM case so the detrimental leakage becomes less of a concern. The degree of mode confinement (shown in Figure 1b) in the slot as compared to the 2D case serves as a good indicator on how close the behavior of the 3D and 2D components will be.

Another viable approach is to utilize a sandwich-type structure for the dielectric slot. Our simulations show that when refraction index of the central region ($80 \times 50 \text{ nm}^2$) in the $w \times h = 80 \times 100 \text{ nm}^2$ dielectric slot is doubled from 1.5 to 3, the energy confinement within the slot region increases to ~ 0.9 . This implies that the interaction between the slot plasmon mode and the metallic edges can be considerably suppressed. Consequently, numerical modeling shows that the power reflection from a dead-end mirror in the sandwich-core slot waveguide reaches above 80%, and the power transmission through a curved bend is over 70%. These values represent a twenty percent improvement in performance over our standard slot waveguides. Similarly, a 4-way splitter in the sandwich-core slot waveguide acts close to a “memoryless” device where an equal output power of ~ 0.25 is transmitted from the X-junction into each channel, regardless of the choice of input port for the incident SPPs.^[22]

To summarize, we have presented an analysis of several passive elements for three-dimensional plasmonic slot waveguides, including mirrors, bends, T-splitters and X-junctions. The possibilities and procedures of optimization of these components are discussed in detail and confirmed with 3D full-wave simulations. The elements discussed in this work represent key building blocks that enable efficient routing of light in future photonic nanocircuits and on-chip optical links.

Acknowledgements

We gratefully acknowledge financial support from the Intel Corporation for this research.

Received: April 16, 2010

Revised: August 10, 2010

Published online: September 21, 2010

- [1] R. Zia, J. A. Schuller, A. Chandran, M. L. Brongersma, *Mater. Today* **2006**, 9, 20.
- [2] H. A. Atwater, *Sci. Am.* **2007**, 296, 56.
- [3] D. K. Gramotnev, S. I. Bozhevolnyi, *Nat. Photonics* **2010**, 4, 83.
- [4] J. A. Schuller, E. S. Barnard, W. Cai, Y. C. Jun, J. S. White, M. L. Brongersma, *Nat. Mater.* **2010**, 9, 193.
- [5] E. N. Economou, *Phys. Rev.* **1969**, 182, 539.
- [6] R. Zia, M. D. Selker, P. B. Catrysse, M. L. Brongersma, *J. Opt. Soc. Am. A* **2004**, 21, 2442.
- [7] G. Veronis, Z. F. Yu, S. E. Kocabas, D. A. B. Miller, M. L. Brongersma, S. H. Fan, *Chin. Opt. Lett.* **2009**, 7, 302.
- [8] M. L. Brongersma, J. W. Hartman, H. A. Atwater, *Phys. Rev. B* **2000**, 62, 16356.

- [9] J. C. Weeber, A. Dereux, C. Girard, J. R. Krenn, J. P. Goudonnet, *Phys. Rev. B* **1999**, *60*, 9061.
- [10] S. I. Bozhevolnyi, V. S. Volkov, E. Devaux, J. Y. Laluet, T. W. Ebbesen, *Nature* **2006**, *440*, 508.
- [11] W. S. Cai, J. S. White, M. L. Brongersma, *Nano Lett.* **2009**, *9*, 4403.
- [12] G. Veronis, S. H. Fan, *Opt. Lett.* **2005**, *30*, 3359.
- [13] L. Liu, Z. H. Han, S. L. He, *Opt. Express* **2005**, *13*, 6645.
- [14] G. Veronis, S. H. Fan, *J. Lightwave Technol.* **2007**, *25*, 2511.
- [15] F. M. Kong, K. Li, B. I. Wu, H. Huang, H. S. Chen, J. A. Kong, *Prog. Electromagn. Res. PIER* **2007**, *76*, 449.
- [16] J. A. Dionne, H. J. Lezec, H. A. Atwater, *Nano Lett.* **2006**, *6*, 1928.
- [17] P. B. Johnson, R. W. Christy, *Phys. Rev. B* **1972**, *6*, 4370.
- [18] G. Veronis, S. H. Fan, *Appl. Phys. Lett.* **2005**, *87*, 131102.
- [19] S. E. Kocabas, G. Veronis, D. A. B. Miller, S. H. Fan, *IEEE J. Select. Topics Quantum Electron.* **2008**, *14*, 1462.
- [20] J. S. Huang, T. Feichtner, P. Biagioni, B. Hecht, *Nano Lett.* **2009**, *9*, 1897.
- [21] S. H. Fan, S. G. Johnson, J. D. Joannopoulos, C. Manolatos, H. A. Haus, *J. Opt. Soc. Am. B* **2001**, *18*, 162.
- [22] E. Feigenbaum, M. Orenstein, *Opt. Express* **2007**, *15*, 17948.